

## Nitro-Functionalized Oligothiophenes as a Novel Type of Electroactive Molecular Material: Spectroscopic, Electrochemical, and Computational Study

Juan Casado,<sup>†,‡</sup> Ted M. Pappenfus,<sup>‡</sup> Larry L. Miller,<sup>\*,‡</sup> Kent R. Mann,<sup>‡</sup> Enrique Ortí,<sup>\*,§</sup> Pedro M. Viruela,<sup>§</sup> Rosendo Pou-Amérgo,<sup>§</sup> Víctor Hernández,<sup>†</sup> and Juan T. López Navarrete<sup>\*,†</sup>

Contribution from the Departamento de Química Física, Facultad de Ciencias, Universidad de Málaga, 29071-Málaga, Spain, Department of Chemistry, University of Minnesota, Minneapolis, Minnesota 55455, and Institut de Ciència Molecular, Universitat de València, 46100-Bujassot (València), Spain

Received July 24, 2002; E-mail: teodomiro@uma.es

**Abstract:** A novel series of terthiophenes bearing electron-donor and electron-acceptor groups at the end  $\alpha$ -positions has been prepared. The analysis of the UV-vis, infrared, and Raman spectra, performed with the aid of density functional theory calculations, shows that the asymmetrically substituted nitro compounds PhT<sub>3</sub>NO<sub>2</sub> and BrT<sub>3</sub>NO<sub>2</sub> behave as push-pull systems and present an intense photoinduced charge transfer in the visible spectrum. The symmetrically substituted dinitro compound NO<sub>2</sub>T<sub>3</sub>NO<sub>2</sub> displays a highly delocalized structure with a low single-double bond length alternation and also displays a low-energy absorption band in the visible region. The novel nitroterthiophenes possess attractive electrochemical properties since they generate stable species both upon oxidation and reduction. Oxidation mainly involves changes in the oligothiophene backbone and leads to the formation of stable cations even for NO<sub>2</sub>T<sub>3</sub>NO<sub>2</sub>. Reduction is mainly nitro-centered but also affects the conjugated structure. Radical anions and dianions are formed for PhT<sub>3</sub>NO<sub>2</sub> and BrT<sub>3</sub>NO<sub>2</sub>. Dianions, not radical anions, and trianions are obtained for NO<sub>2</sub>T<sub>3</sub>NO<sub>2</sub>. Nitro-functionalized terthiophenes are shown to be very promising as electroactive molecular materials since they behave as push-pull systems, present a very intense photoinduced charge transfer in the visible region, and could act as both n- and p-channel conductors in organic electronic transistors.

### I. Introduction

Materials based on  $\pi$ -conjugated organic compounds are promising candidates for new technologies since they are characterized by relevant electrical and optical properties with potential applications in electronics,<sup>1-3</sup> optoelectronics,<sup>4,5</sup> and information-storage devices.<sup>6,7</sup> Polythiophene has been extensively studied as the prototype polymer in the field of  $\pi$ -conjugated materials. The intrinsic physical properties of polythiophene are of great interest, even though they are often limited by structural and chemical disorder.<sup>8,9</sup> Oligothiophenes

have been shown to be suitable models for understanding the electronic structure and the optical properties of the polymer.<sup>10</sup> The synthesis of oligothiophenes with well-defined substitution patterns and chain lengths constitutes a very useful strategy to obtain molecular materials in which the electrical and optical responses can be tuned by making appropriate modifications of the chemical structure.<sup>10</sup>

The ability of oligothiophenes to behave as chromophores and redox-active molecules is related, among other factors, to the efficiency of the intramolecular delocalization of the  $\pi$ -electrons.<sup>10,11</sup> Oligothiophenes bearing a donor group and an acceptor group at the end  $\alpha$ -positions can behave as push-pull systems, with a highly polarizable  $\pi$ -electron system, when exposed to moderately strong electric or electromagnetic fields. Push-pull oligothiophenes yield materials with interesting

<sup>†</sup> Universidad de Málaga.

<sup>‡</sup> University of Minnesota.

<sup>§</sup> Universitat de València.

- (1) Katz, H. E.; Bao, Z.; Gilat, S. L. *Acc. Chem. Res.* **2001**, *34*, 359.
- (2) (a) Crone, B.; Dodabalapur, A.; Llin, Y.-Y.; Filas, R. W.; Bao, Z.; LaDuca, A.; Sarpeshkar, R.; Katz, H. E. *Nature* **2000**, *403*, 521. (b) Marder, S. R.; Kippelen, B.; Jen, A. K.-Y.; Peyghambarian, N. *Nature* **1997**, *388*, 845.
- (3) (a) Schoonveld, W. A.; Wildeman, J.; Fichou, D.; Bobbert, P. A.; van Wees, B. J.; Klapwijk, T. M. *Nature* **2000**, *404*, 977. (b) Dimitrakopoulos, C. D.; Malenfant, P. R. L. *Adv. Mater.* **2002**, *14*, 99.
- (4) (a) Makinen, A. J.; Hill, I. G.; Noda, T.; Shirota, Y.; Kafati, Z. H. *Appl. Phys. Lett.* **2001**, *78*, 670. (b) Noda, T.; Ogawa, H.; Noma, N.; Shirota, Y. *Appl. Phys. Lett.* **1997**, *70*, 699. (c) Noda, T.; Ogawa, H.; Noma, N.; Shirota, Y. *J. Mater. Chem.* **1999**, *9*, 2177. (d) Schon, J. H.; Kloc, Ch, Laudise, R. A.; Batlogg, B. *Phys. Rev. B* **1998**, *58*, 12952.
- (5) Fichou, D. *J. Mater. Chem.* **2000**, *10*, 571.
- (6) (a) Tour, J. M. *Acc. Chem. Res.* **2000**, *33*, 791. (b) Cassel, A. M.; Lee Asplund, C.; Tour, J. M. *Angew. Chem., Int. Ed.* **1999**, *38*, 2403.
- (7) Wurthner, F. *Angew. Chem., Int. Ed.* **2001**, *40*, 1037.

- (8) (a) *Handbook of Conducting Polymers*, 2nd ed.; Skotheim, T. A., Elsenbaumer, R. L., Reynolds, J. R., Eds.; Marcel Dekker: New York, 1998. (b) *Conjugated Polymers and Related Materials*; Salaneck, W. R., Lundstrom, I., Ranby, B., Eds.; Oxford University Press: Oxford, U.K., 1993.
- (9) (a) Chen, T. A.; Wu, X.; Rieke, R. R. *J. Am. Chem. Soc.* **1995**, *117*, 233. (b) Zhang, F.; Svensson, M.; Andersson, M. A.; Maggini, M.; Bucella, S.; Menna, E.; Inganas, O. *Adv. Mater.* **2001**, *13*, 1871.
- (10) (a) *Electronic Materials: The Oligomeric Approach*; Müllen, K., Wegner, G., Eds.; Wiley-VCH: Weinheim, Germany, 1998. (b) *Handbook of Oligo- and Polythiophenes*; Fichou, D., Ed.; Wiley-VCH: New York, 1999.
- (11) Balakina, M. Y.; Li, J.; Geskin, V. M.; Marder, S. R.; Brédas, J. L. *J. Chem. Phys.* **2000**, *113*, 9598.

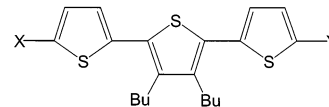
nonlinear optical properties and, in particular, high second-order polarizabilities.<sup>12</sup> These properties result from the existence of a photoinduced intramolecular charge transfer at relatively low energies, which depends on the efficiency of the  $\pi$ -electron delocalization along the  $\pi$ -conjugated spacer and on the strength of the electron-donor and electron-acceptor end groups.<sup>11,12</sup> The attachment of these electronically active end groups to the  $\pi$ -conjugated backbone gives rise to sizable changes of the structural and electronic properties.

The analysis of the equilibrium geometries, UV-vis and vibrational spectra, and electrochemical behavior of this kind of molecular material provides useful information on their structure and electronic properties. The effective conjugation coordinate (ECC) model developed by Zerbi's group<sup>13-15</sup> is of crucial relevance in the understanding of the vibrational spectra of  $\pi$ -conjugated materials in different redox states. The usefulness of this approach lies in the capability of estimating the mean length for  $\pi$ -electron delocalization from the analysis of the frequency behavior of the selectively enhanced Raman bands associated to the so-called ECC mode.<sup>15-17</sup> Particular attention has been paid over the past few years to the theoretical analysis of the electronic and vibrational spectra within the framework of density functional theory (DFT).<sup>18-21</sup> The successful performance of this approach for computing spectroscopic properties is well-established. The method has been shown to yield reliable predictions and interpretations of the electronic and vibrational spectra of many organic molecules.

This article reports the synthesis of novel  $\alpha,\alpha'$ -terthiophenes end-capped with phenyl, bromine, and/or nitro groups (see Figure 1 for chemical structures). The central thiophene ring is substituted with *n*-butyl chains to enhance the solubility of the systems. UV-vis, infrared, and Raman spectra are analyzed, assigned, and interpreted with the help of DFT calculations. Our main goal is to obtain detailed information on the molecular structure and on the electronic, optical, and redox properties of the compounds synthesized. Special attention is paid to investigate the efficiency of  $\pi$ -electron delocalization and intramolecular charge transfer.

## II. Experimental Section

(a) **Syntheses.** The syntheses of PhT<sub>3</sub>Ph,<sup>22a</sup> PhT<sub>3</sub>Br,<sup>22b</sup> BrT<sub>3</sub>Br,<sup>22c</sup> and NO<sub>2</sub>T<sub>3</sub>NO<sub>2</sub><sup>22c</sup> were carried out following previously reported procedures. The nitration was performed with a "claycop" reagent and



X	Y	Compound
H	H	HT <sub>3</sub> H
Ph	Ph	PhT <sub>3</sub> Ph
Ph	Br	PhT <sub>3</sub> Br
Br	Br	BrT <sub>3</sub> Br
Ph	NO <sub>2</sub>	PhT <sub>3</sub> NO <sub>2</sub>
Br	NO <sub>2</sub>	BrT <sub>3</sub> NO <sub>2</sub>
NO <sub>2</sub>	NO <sub>2</sub>	NO <sub>2</sub> T <sub>3</sub> NO <sub>2</sub>

**Figure 1.** Chemical structure of the terthiophenes (XT<sub>3</sub>Y) studied in this work.

procedures similar to those published in the literature.<sup>23</sup> <sup>1</sup>H NMR spectra were recorded on a Varian VXR-300 MHz instrument. The chemical shifts are given in parts per million (ppm) and referenced to the residual chloroform peak (7.26 ppm). Mass spectra were obtained on a Finnigan MAT 95 or VG 7070E-HF mass spectrometer.

**3',4'-Dibutyl-5-nitro-5''-phenyl-2,2':5',2''-terthiophene (PhT<sub>3</sub>NO<sub>2</sub>).** In a 50 mL round-bottom flask, 1.27 g (2.90 mmol) of 3',4'-dibutyl-5-phenyl-2,2':5',2''-terthiophene (PhT<sub>3</sub>) was dissolved in 25 mL of carbon tetrachloride and 6.25 mL of acetic anhydride. To this solution was added 1.08 g of "claycop" reagent (2.68 mmol/g), and the reaction mixture was stirred at room temperature for 18 h. The reaction mixture was filtered and the filter was washed with methylene chloride. The combined organic solutions were washed with water (2 × 15 mL), dried with MgSO<sub>4</sub>, and concentrated. The crude oil was purified by silica gel flash chromatography (25% dichloromethane in hexanes followed by 50% dichloromethane in hexanes) to provide 0.57 g (41%) of PhT<sub>3</sub>NO<sub>2</sub> as a deep red solid. <sup>1</sup>H NMR (300 MHz, CDCl<sub>3</sub>)  $\delta$  7.90 (d, 1H,  $J_{4,3}$  = 4.5 Hz), 7.63 (m, 2H), 7.41 (m, 2H), 7.31 (m, 1H), 7.30 (d, 1H,  $J_{4',3''}$  = 3.9 Hz), 7.16 (d, 1H,  $J_{3',4''}$  = 3.9 Hz), 7.08 (d, 1H,  $J_{3,4}$  = 4.5 Hz), 2.78 (m, 4H), 1.51 (m, 8H), 0.99 (m, 6H). HREIMS calcd 481.1204, found 481.1203 (M<sup>+</sup>).

**5-Bromo-3',4'-dibutyl-5''-nitro-2,2':5',2''-terthiophene (BrT<sub>3</sub>NO<sub>2</sub>).** In a 250 mL round-bottom flask equipped with an addition funnel, 3.00 g (7.40 mmol) of 3',4'-dibutyl-5-nitro-2,2':5',2''-terthiophene and 75 mL of 1:1 acetic acid/chloroform mixture were added. The system was purged with nitrogen and cooled to 0 °C. NBS (1.32 g, 7.40 mmol) was dissolved in 15 mL of acetone and transferred to the addition funnel. The NBS solution was added dropwise with stirring over 1.5 h. The reaction was allowed to slowly warm to room temperature overnight. Water (20 mL) was added, and the organics were washed with NaHCO<sub>3</sub> solution and dried with MgSO<sub>4</sub>. The crude oil was purified by silica gel flash chromatography (25% dichloromethane in hexanes) to provide 1.45 g (40%) of BrT<sub>3</sub>NO<sub>2</sub> as a deep red solid. <sup>1</sup>H NMR (300 MHz, CDCl<sub>3</sub>)  $\delta$  7.89 (d, 1H,  $J_{4',3''}$  = 4.5 Hz), 7.06 (d, 1H,  $J_{4,3}$  = 3.9 Hz), 7.05 (d, 1H,  $J_{3',4''}$  = 4.5 Hz), 6.92 (d, 1H,  $J_{3,4}$  = 3.9 Hz), 2.75 (t, 2H), 2.67 (t, 2H), 1.49 (m, 8H), 0.97 (m, 6H). HRFABMS calcd 483.9996, 484.9976; found 483.0008, 485.0005 (M<sup>+</sup>).

(b) **Electrochemistry.** Cyclic voltammetry was carried out at room temperature with a scan rate of 100 mV/s in a 0.1 M tetrabutylammonium hexafluorophosphate (TBAPF<sub>6</sub>) solution in dichloromethane. A 0.053 M concentration was used, in all cases, for the molecules under study. A glassy carbon electrode and a platinum electrode were employed as working and auxiliary electrodes, respectively. An Ag/AgCl electrode was used as reference.

- (12) (a) Effenberger, F.; Würthner, F.; Steybe, F. *J. Org. Chem.* **1995**, *60*, 2082. (b) Higuchi, H.; Nakayama, T.; Koyama, H.; Ojima, J.; Wada, T.; Sasabe, H. *Bull. Chem. Soc. Jpn.* **1995**, *68*, 2363. (c) Higuchi, H.; Uraki, Y.; Yokota, H.; Koyama, H.; Ojima, J.; Wada, T.; Sasabe, H. *Bull. Chem. Soc. Jpn.* **1998**, *71*, 483. (d) Hernández, V.; Casado, J.; Effenberger, F.; López Navarrete, J. T. *J. Chem. Phys.* **2000**, *112*, 5105.
- (13) Castiglioni, C.; López Navarrete, J. T.; Gussoni, M.; Zerbi, G. *Solid State Commun.* **1988**, *65*, 625.
- (14) Zerbi, G.; Castiglioni, C.; López Navarrete, J. T.; Tian, B.; Gussoni, M. *Synth. Met.* **1989**, *28*, D359.
- (15) Del Zoppo, M.; Castiglioni, C.; Zuliani, P.; Zerbi, G. In ref 8a, p 765.
- (16) (a) Casado, J.; Hotta, S.; Hernández, V.; López Navarrete, J. T. *J. Phys. Chem. A* **1999**, *103*, 816. (b) Hernández, V.; Casado, J.; Ramírez, F. J.; Zotti, G.; Hotta, S.; López Navarrete, J. T. *J. Chem. Phys.* **1996**, *104*, 9271.
- (17) Agosti, E.; Rivola, M.; Hernández, V.; Del Zoppo, M.; Zerbi, G. *Synth. Met.* **1999**, *100*, 101.
- (18) (a) Wiberg, K. B.; Stratmann, R. E.; Frisch, M. J. *Chem. Phys. Lett.* **1998**, *297*, 60. (b) Stratmann, R. E.; Scuseria, G. E.; Frisch, M. J. *J. Chem. Phys.* **1998**, *109*, 8218. (c) Hirata, S.; Lee, T. J.; Head-Gordon, M. *J. Chem. Phys.* **1999**, *111*, 8904. (d) Hsu, C.-P.; Hirata, S.; Head-Gordon, M. *J. Phys. Chem. A* **2001**, *105*, 451.
- (19) Casado, J.; Miller, L. L.; Mann, K. R.; Pappenfus, T. M.; Kanemitsu, Y.; Ortí, E.; Viruela, P. M.; Pou-Amérgo, R.; Hernández, V.; López-Navarrete, J. T. *J. Phys. Chem. B* **2002**, *106*, 3872.
- (20) Stephens, P. J.; Devlin, F. J.; Chabalowski, C. F.; Frisch, M. J. *J. Phys. Chem.* **1994**, *98*, 11623.
- (21) Scott, A. P.; Radom, L. *J. Phys. Chem.* **1996**, *100*, 16502.

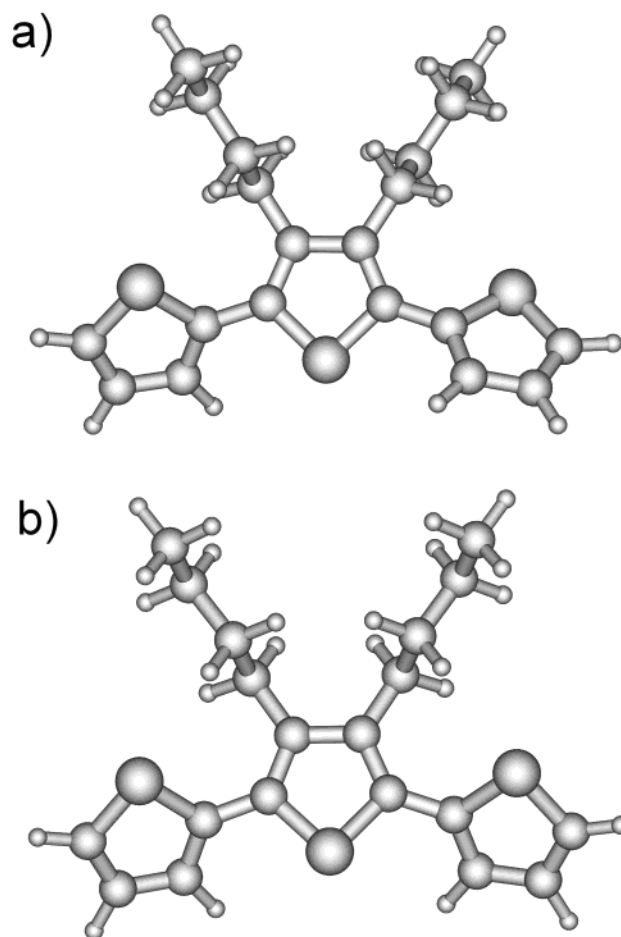
- (22) (a) Graf, D. D.; Campbell, J. P.; Mann, K. R.; Miller, L. L. *J. Am. Chem. Soc.* **1996**, *118*, 5480. (b) Pappenfus, T. M.; Mann, K. R. *Org. Lett.* **2002**, *4*, 3403. (c) Pappenfus, T. M.; Raff, J. D.; Hukkanen, E. J.; Burney, J.; Casado, J.; Drew, S. M.; Miller, L. L.; Mann, K. R. *J. Org. Chem.* **2002**, *67*, 6015.
- (23) Gigante, B.; Prazeres, A. O.; Marcelo-Curto, M. J. *J. Org. Chem.* **1995**, *60*, 3445.

(c) **Optical Spectra.** UV–vis spectra were recorded for dichloromethane solutions with a Perkin-Elmer Lambda 19 spectrometer. Extinction coefficients were calculated from experimentally determined absorbances by use of Lambert–Beer’s law. Infrared absorption spectra were registered for pressed KBr pellets with a Perkin-Elmer FTIR spectrometer, model 1760 X, purged with dry Ar gas. FT-Raman spectra were measured by use of the FT-Raman accessory kit (FRA/106-S) of a Bruker Equinox 55 FT-IR interferometer. A continuous-wave Nd:YAG laser working at 1064 nm was employed for Raman excitation.

(d) **Computational Methods.** Density functional theory (DFT) calculations were carried out with the A.7 revision of the GAUSSIAN 98 program package<sup>24</sup> running on SGI Origin 2000 computers and IBM RS/6000 workstations. All the calculations including geometry optimizations, electronic excitation energies, and vibrational spectra were performed on isolated systems with Becke’s three-parameter B3LYP exchange-correlation functional.<sup>25</sup> The 6-31G\*\* basis set<sup>26</sup> was chosen as a compromise between accuracy and applicability to large molecules. The calculated harmonic vibrational frequencies were uniformly scaled by a factor of 0.96 as recommended by Scott and Radom.<sup>21</sup> All the theoretical vibrational data quoted in the text are thus scaled values. Vertical electronic excitation energies were computed by the time-dependent DFT (TDDFT) approach.<sup>27,28</sup> The 12 lowest-energy electronic excited states were at least computed for all the compounds. Numerical applications reported so far indicated that TDDFT employing current exchange-correlation functionals performs significantly better than HF-based single excitations theories for the low-lying valence excited states of both closed-shell and open-shell molecules.<sup>18,29</sup>

### III. Results and Discussion

(a) **Optimized Geometries.** 3',4'-Dibutyl-2,2':5',2''-terthiophene (HT<sub>3</sub>H) was first calculated as a reference molecule for comparison purposes. The geometry of HT<sub>3</sub>H was optimized under different symmetry restrictions both for trans and cis conformations. The minimum-energy conformation corresponds to the transoid *C*<sub>2</sub> structure depicted in Figure 2a, for which the *n*-butyl side chains are fully extended and lie above and below the plane of the central thiophene ring to minimize the steric crowding. At the B3LYP/6-31G\*\* level, the *C*<sub>2</sub> structure is predicted to be 0.88 kcal/mol more stable than the *C*<sub>s</sub> conformation sketched in Figure 2b, for which both *n*-butyl chains lie on the same side of the thiophene plane. The *C*<sub>s</sub> conformation is, however, the structure observed in the crystal because it leads to a more compact crystal packing.<sup>30</sup> The dihedral angles between adjacent thiophene rings (S–C–C–S



**Figure 2.** B3LYP/6-31G\*\* minimum-energy conformations calculated for HT<sub>3</sub>H. (a) *C*<sub>2</sub> symmetry; (b) *C*<sub>s</sub> symmetry.

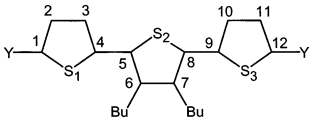
angles) calculated for the *C*<sub>2</sub> (141.7°) and *C*<sub>s</sub> (141.3°) conformations are slightly larger than those observed in the crystal (~147°).

The transoid *C*<sub>2</sub> conformation was also calculated to be more stable than the *C*<sub>s</sub> conformation by ~0.90 kcal/mol for the symmetrically disubstituted terthiophenes PhT<sub>3</sub>Ph, BrT<sub>3</sub>Br, and NO<sub>2</sub>T<sub>3</sub>NO<sub>2</sub>. The dihedral angles between adjacent thiophene rings change from 141.9° in BrT<sub>3</sub>Br to 145.1° in PhT<sub>3</sub>Ph to 152.6° in NO<sub>2</sub>T<sub>3</sub>NO<sub>2</sub>. For PhT<sub>3</sub>Ph, the *C*<sub>s</sub>-type structure observed in the crystal presents dihedral angles of ~150°.<sup>31</sup> For NO<sub>2</sub>T<sub>3</sub>NO<sub>2</sub>, the sulfur atoms in adjacent thiophene rings adopt a cis orientation in the crystal.<sup>22c</sup> The cisoid *C*<sub>s</sub> structure was, however, calculated to be 1.79 kcal/mol less stable than the transoid *C*<sub>2</sub> structure for the isolated molecule. Transoid conformations similar to that sketched in Figure 2a were also obtained for the asymmetric derivatives PhT<sub>3</sub>Br, PhT<sub>3</sub>NO<sub>2</sub>, and BrT<sub>3</sub>NO<sub>2</sub> as the most stable conformations.

Table 1 summarizes the B3LYP/6-31G\*\*-optimized bond lengths for the terthiophene skeleton of HT<sub>3</sub>H, taken as a reference, and for the six derivatives studied in this work. Only the values calculated for the most stable *C*<sub>2</sub>-type transoid conformation are given. The X-ray distances reported for NO<sub>2</sub>T<sub>3</sub>NO<sub>2</sub> are also included in Table 1.<sup>22c</sup> The attachment of phenyl groups causes a slight lengthening (shortening) of the C=C (C–C) bonds of the outer thiophene rings, while the central rings

- (24) Frisch, M. J.; Trucks, G. W.; Schlegel, H. B.; Scuseria, G. E.; Robb, M. A.; Cheeseman, J. R.; Zakrzewski, V. G.; Montgomery, J. A.; Stratman, R. E.; Burant, J. C.; Dapprich, S.; Millam, J. M.; Daniels, A. D.; Kudin, K. N.; Strain, M. C.; Farkas, O.; Tomasi, J.; Barone, V.; Cossi, M.; Cammi, R.; Mennucci, B.; Pomelli, C.; Adamo, C.; Clifford, S.; Ochterski, J.; Petersson, G.; Ayala, P. Y.; Cui, Q.; Morokuma, K.; Malick, D. K.; Rabuck, A. D.; Raghavachari, K.; Foresman, J. B.; Cioslowski, J.; Ortiz, J. V.; Baboul, A. G.; Stefanov, B. B.; Liu, G.; Liashenko, A.; Piskorz, P.; Komaromi, I.; Gomperts, R.; Martin, R. L.; Fox, D. J.; Keith, T.; Al-Laham, M. A.; Peng, C. Y.; Manayakkara, A.; Gonzalez, C.; Challacombe, M.; Gill, P. M. W.; Johnson, B. G.; Chen, W.; Wong, M. W.; Andres, J. L.; Head-Gordon, M.; Replogle, E. S.; Pople, J. A. *Gaussian 98*, Revision A.7; Gaussian, Inc.: Pittsburgh, PA, 1998.
- (25) Becke, A. D. *J. Chem. Phys.* **1993**, *98*, 1372.
- (26) Francl, M. M.; Pietro, W. J.; Hehre, W. J.; Binkley, J. S.; Gordon, M. S.; Defrees, D. J.; Pople, J. A. *J. Chem. Phys.* **1982**, *77*, 3654.
- (27) (a) Runge, E.; Gross, E. K. U. *Phys. Rev. Lett.* **1984**, *52*, 997. (b) Gross, E. K. U.; Kohn, W. *Adv. Quantum Chem.* **1990**, *21*, 255. (c) Gross, E. K. U.; Ullrich, C. A.; Gossmann, U. *J. Density Functional Theory*; Gross, E. K. U., Driessler, R. M., Eds.; Plenum Press: New York, 1995; p 149.
- (28) Casida, M. E. *Recent Advances in Density Functional Methods, Part I*; Chong, D. P., Ed.; World Scientific: Singapore, 1995; p 155.
- (29) Koch, W.; Holthausen, M. C. *A Chemist's Guide to Density Functional Theory*; Wiley-VCH: Weinheim, Germany, 2000.
- (30) DeWitt, L.; Blanchard, J. L.; LeGoff, E.; Benz, M. E.; Liao, J. H.; Kanatzidis, M. G. *J. Am. Chem. Soc.* **1993**, *115*, 12158.

- (31) Graf, D. D.; Duan, R. G.; Campbell, J. P.; Miller, L. L.; Mann, K. R. *J. Am. Chem. Soc.* **1997**, *119*, 5888.

**Table 1.** Selected B3LYP/6-31G\*\*-Optimized Bond Distances and Dihedral Angles for XT<sub>3</sub>Y Terthiophenes<sup>a</sup>


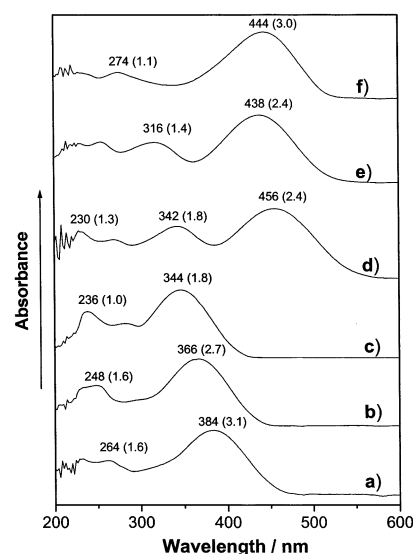
parameter	HT <sub>3</sub> H	PhT <sub>3</sub> Ph	PhT <sub>3</sub> Br	BrT <sub>3</sub> Br	PhT <sub>3</sub> NO <sub>2</sub>	BrT <sub>3</sub> NO <sub>2</sub>	NO <sub>2</sub> T <sub>3</sub> NO <sub>2</sub> <sup>b</sup>
C1–C2	1.368	1.378	1.378	1.366	1.378	1.367	1.373 (1.361)
C2–C3	1.423	1.416	1.417	1.423	1.416	1.422	1.410 (1.403)
C3–C4	1.380	1.382	1.381	1.379	1.382	1.380	1.391 (1.378)
C4–C5	1.457	1.454	1.455	1.456	1.454	1.455	1.452 (1.456)
C5–C6	1.385	1.386	1.386	1.385	1.389	1.387	1.390 (1.384)
C6–C7	1.441	1.440	1.440	1.440	1.437	1.438	1.437 (1.437)
C7–C8			1.385		1.390	1.390	
C8–C9			1.456		1.449	1.450	
C9–C10			1.380		1.392	1.392	
C10–C11			1.423		1.409	1.409	
C11–C12			1.366		1.373	1.373	
C1–X	1.081	1.467	1.467	1.884	1.466	1.882	1.430 (1.423)
C12–Y			1.884		1.426	1.427	
S1–C1	1.733	1.752	1.752	1.737	1.752	1.737	1.735 (1.717)
S1–C4	1.759	1.757	1.757	1.763	1.757	1.762	1.755 (1.738)
S2–C5	1.751	1.752	1.752	1.751	1.750	1.748	1.750 (1.730)
S2–C8			1.751		1.754	1.754	
S3–C9			1.763		1.757	1.756	
S3–C12			1.738		1.736	1.736	
S1–C4–C5–S2	141.7	145.1	144.2	141.9	147.5	143.5	152.6
S3–C9–C8–S2			142.9		156.5	155.2	

<sup>a</sup> Bond distances are given in angstroms; dihedral angles are given in degrees. X = Y compounds have C<sub>2</sub> symmetry. <sup>b</sup> Average X-ray bond distances from ref 22c are given in parentheses.

remain almost unaffected. The extension of the  $\pi$ -conjugation to the phenyl end-caps seems to be the most feasible explanation for this geometry relaxation. Bromination of the end  $\alpha, \alpha'$ -positions does not affect the molecular geometry of the  $\pi$ -conjugated spine. The structure of PhT<sub>3</sub>Br is halfway between those of PhT<sub>3</sub>Ph and BrT<sub>3</sub>Br. The geometries of the phenyl and bromine environments are very close to those calculated for PhT<sub>3</sub>Ph and BrT<sub>3</sub>Br, respectively. It can therefore be concluded that these three derivatives display molecular structures with a strong aromatic character, as in HT<sub>3</sub>H. The degree of bond length alternation (BLA), calculated as the difference between the average lengths of the C–C and C=C bonds of the  $\pi$ -conjugated path, amounts to 0.063 Å for HT<sub>3</sub>H, 0.054 Å for PhT<sub>3</sub>Ph, 0.058 Å for PhT<sub>3</sub>Br, and 0.063 Å for BrT<sub>3</sub>Br.

Upon nitroencapsulation, sizable lengthenings of the C=C bonds (up to +0.011 Å for C3=C4) and shortenings of the C–C bonds (up to –0.013 Å for C2–C3) take place for NO<sub>2</sub>T<sub>3</sub>NO<sub>2</sub>. The molecular structure of the  $\pi$ -conjugated backbone changes from the typical aromatic pattern of HT<sub>3</sub>H to a partially quinonoid-like pattern in which the degree of bond alternation is drastically reduced. The overall BLA has a value of 0.047 Å, which goes down to 0.028 Å if only the C=C and C–C bond lengths of the outermost thiophene rings are taken into account in the average difference. The calculated bond distances are in good agreement with the experimental X-ray values (see Table 1), the average deviation being only 0.007 Å for the CC conjugated path.

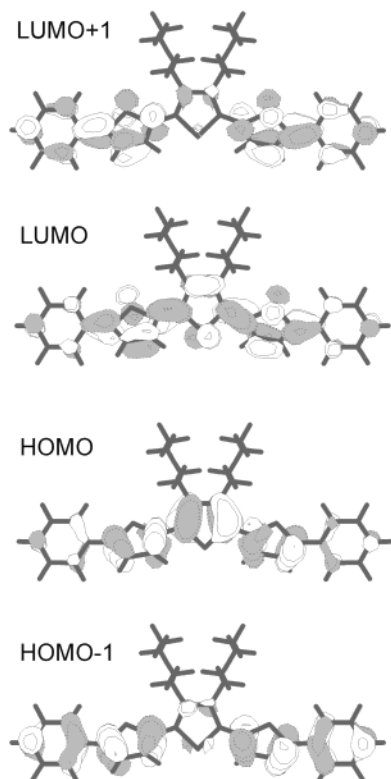
For PhT<sub>3</sub>NO<sub>2</sub>, the strength of the electron-withdrawing NO<sub>2</sub> group mainly affects the ring to which this group is attached, the geometrical changes being even more pronounced than those predicted for NO<sub>2</sub>T<sub>3</sub>NO<sub>2</sub>. The partial quinoidization of the acceptor subunit readily decreases upon going to the center of the molecule, and the geometry of the phenyl subunit is similar to those of PhT<sub>3</sub>Ph. The overall BLA value for PhT<sub>3</sub>NO<sub>2</sub> is



**Figure 3.** UV–vis spectra recorded in CH<sub>2</sub>Cl<sub>2</sub> solution for (a) PhT<sub>3</sub>Ph, (b) PhT<sub>3</sub>Br, (c) BrT<sub>3</sub>Br, (d) PhT<sub>3</sub>NO<sub>2</sub>, (e) BrT<sub>3</sub>NO<sub>2</sub>, and (f) NO<sub>2</sub>T<sub>3</sub>NO<sub>2</sub>.  $\lambda_{\text{max}}$  values (in nanometers) are quoted for the main absorption bands. In parentheses, the molar absorptivity values ( $10^4 \text{ M}^{-1} \text{ cm}^{-1}$ ) are shown.

0.049 Å and decreases to 0.026 and 0.036 Å for the nitro and phenyl subunits, respectively. The case of BrT<sub>3</sub>NO<sub>2</sub> resembles that of PhT<sub>3</sub>NO<sub>2</sub>. The NO<sub>2</sub> subunit displays certain degree of quinonoid-like character, while the geometry of the bromine subunit is similar to those of BrT<sub>3</sub>Br or HT<sub>3</sub>H. The generation of two different molecular domains within the  $\pi$ -conjugated bridge (one with a partial quinonoid-like character and the other with an almost pure aromatic-like character) has been previously reported for push–pull oligothiophenes.<sup>12d</sup>

**(b) Electronic Spectra.** Figure 3 displays the UV–vis spectra recorded in dichloromethane solution for the end-capped  $\alpha, \alpha'$ -



**Figure 4.** Electronic density contours ( $0.03 \text{ e/bohr}^3$ ) calculated with the Molden-4 graphics interface for selected molecular orbitals of  $\text{PhT}_3\text{Ph}$ .

terthiophenes studied in this work. Noticeable differences in the values of  $\lambda_{\text{max}}$ , as well as in the number of bands, are seen in the electronic spectra of these oligomers.  $\text{PhT}_3\text{Ph}$ ,  $\text{PhT}_3\text{Br}$ , and  $\text{BrT}_3\text{Br}$  present one absorption band around 250 nm and a more intense band above 300 nm, which blue-shifts as the phenyl rings are substituted by bromine atoms ( $\text{PhT}_3\text{Ph}$ , 384 nm;  $\text{PhT}_3\text{Br}$ , 366 nm;  $\text{BrT}_3\text{Br}$ , 344 nm). The nitroterthiophenes  $\text{PhT}_3\text{NO}_2$  and  $\text{BrT}_3\text{NO}_2$  also exhibit the absorption band about 250 nm and the band above 300 nm (342 and 316 nm, respectively); however, the most intense absorption now corresponds to a third band that appears around 450 nm ( $\text{PhT}_3\text{NO}_2$ , 456 nm;  $\text{BrT}_3\text{NO}_2$ , 438 nm). The dinitro  $\text{NO}_2\text{T}_3\text{NO}_2$  oligomer only presents the bands at 274 and 444 nm.

To rationalize the evolution of the optical absorption properties with substitution, the electronic spectra of the six end-capped terthiophenes were calculated at the B3LYP/6-31G\*\* level by the TDDFT approach. Starting with  $\text{PhT}_3\text{Ph}$ , TDDFT calculations predict two intense electronic transitions at 3.19 and 4.30 eV with oscillator strengths ( $f$ ) of 1.13 and 0.50, respectively. The transition at 3.19 eV corresponds to the transition to the first excited state ( $1^1\text{A} \rightarrow 1^1\text{B}$ ) and is mainly described by a one-electron excitation from the highest occupied molecular orbital (HOMO) to the lowest unoccupied molecular orbital (LUMO). As sketched in Figure 4, these orbitals are of  $\pi$  nature and are mainly concentrated on the terthiophene backbone. The nature of the transition is thus equivalent to that calculated for the lowest-energy  $\pi-\pi^*$  transition of unsubstituted terthiophene.<sup>32,33</sup> The intense absorption observed at 384 nm (3.23 eV) is therefore assigned to the HOMO  $\rightarrow$  LUMO one-electron

promotion calculated at 3.19 eV. The second band at 264 nm (4.70 eV) is attributed to the transition to the  $2^1\text{B}$  state calculated at 4.30 eV, which mainly results from the HOMO  $- 1 \rightarrow$  LUMO  $+ 1$  excitation. These orbitals are mainly concentrated on the lateral thiophene rings with large contributions from the outer phenyl rings (see Figure 4).

Substitution of phenyl rings by bromine atoms in  $\text{PhT}_3\text{Ph}$  blue-shifts the absorption bands to 366 and 248 nm (3.39 and 5.00 eV) for  $\text{PhT}_3\text{Br}$  and to 344 and 236 nm (3.60 and 5.25 eV) for  $\text{BrT}_3\text{Br}$ . B3LYP/6-31G\*\* calculations also predict this shift to higher energies. The most intense band is calculated at 3.37 ( $f = 0.91$ ) and 3.62 eV ( $f = 0.62$ ) for  $\text{PhT}_3\text{Br}$  and  $\text{BrT}_3\text{Br}$ , respectively, in good accord with the experimental energies. The second intense band is obtained at 4.62 ( $f = 0.33$ ) and 4.95 eV ( $f = 0.23$ ), respectively, underestimating the experimental energy by 0.3–0.4 eV as for  $\text{PhT}_3\text{Ph}$ . The absorption bands observed originate in the HOMO  $\rightarrow$  LUMO and HOMO  $- 1 \rightarrow$  LUMO  $+ 1$  excitations, respectively, as for  $\text{PhT}_3\text{Ph}$ . The shift to higher energies can be easily understood on the basis of the stabilization of the HOMO and HOMO  $- 1$  orbitals as bromine atoms are added (see Figure 5). These atoms largely contribute to the HOMO and HOMO  $- 1$  and show almost no contribution to the LUMO and LUMO  $+ 1$ .

Calculations predict a third transition for  $\text{PhT}_3\text{Ph}$  (3.91 eV),  $\text{PhT}_3\text{Br}$  (4.11 eV), and  $\text{BrT}_3\text{Br}$  (4.33 eV) with a smaller intensity ( $f = 0.05\text{--}0.07$ ), which corresponds to a combination of the HOMO  $- 1 \rightarrow$  LUMO and HOMO  $\rightarrow$  LUMO  $+ 1$  excitations. This transition accounts for the low-intensity band found experimentally at 280 nm (4.43 eV) for  $\text{BrT}_3\text{Br}$  (see Figure 3c) and is not observed for  $\text{PhT}_3\text{Ph}$  and  $\text{PhT}_3\text{Br}$  because it is hidden under the tail of the most intense band.

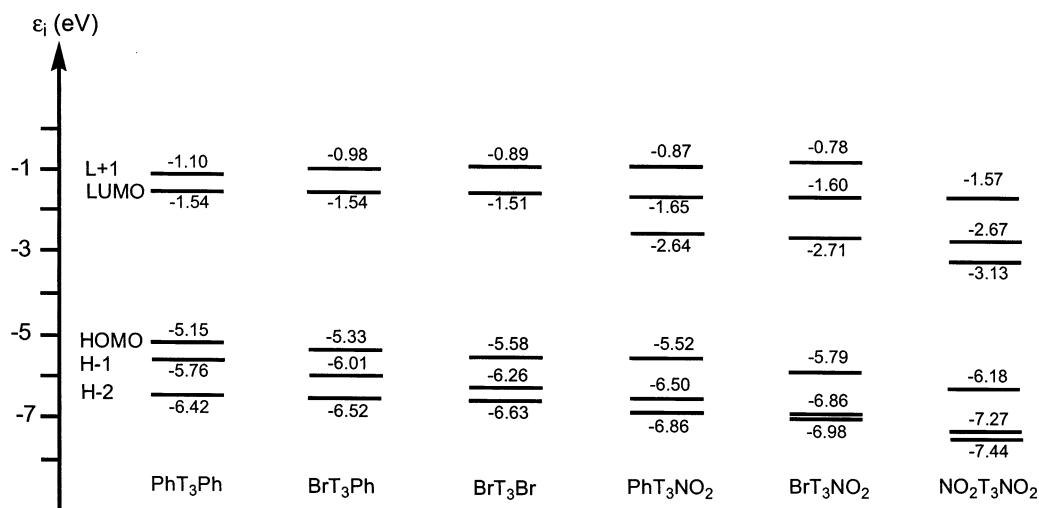
The introduction of the nitro substituents has important consequences for the atomic orbital compositions and energies of the frontier molecular orbitals. The HOMO of  $\text{PhT}_3\text{NO}_2$  is similar to that of  $\text{PhT}_3\text{Ph}$  but the contribution of the thiophene ring linked to the  $\text{NO}_2$  group is smaller (cf. Figures 4 and 6a). By contrast, the LUMO of  $\text{PhT}_3\text{NO}_2$  is concentrated on the  $\text{NO}_2$ -substituted ring. The LUMO is calculated at  $-2.64$  eV, i.e., 1.10 eV lower in energy than the LUMO of  $\text{PhT}_3\text{Ph}$  (see Figure 5). The LUMO and LUMO  $+ 1$  of  $\text{PhT}_3\text{Ph}$  actually correlate with the LUMO  $+ 1$  and LUMO  $+ 2$  of  $\text{PhT}_3\text{NO}_2$ . These changes in the molecular orbital distribution determine important differences in the optical properties of  $\text{PhT}_3\text{NO}_2$ :

(i) The transition to the first excited state associated with the HOMO  $\rightarrow$  LUMO excitation is calculated to be very low in energy at 2.62 eV. This transition is the most intense ( $f = 0.72$ ) and implies an electron density transfer from the left side of the thiophene backbone, including the phenyl ring acting as the electron donor, to the right side of the backbone, including the electron-withdrawing  $\text{NO}_2$  group (see Figure 6a).

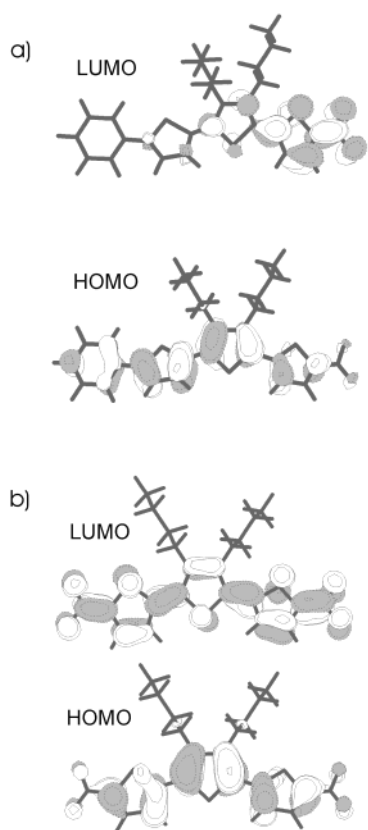
The  $\text{PhT}_3\text{NO}_2$  molecule thus behaves as a push–pull system. The HOMO  $\rightarrow$  LUMO transition accounts for the new intense absorption that  $\text{PhT}_3\text{NO}_2$  shows at 456 nm (2.72 eV), which, on the basis of the theoretical results, corresponds to a charge-transfer absorption band. This charge-transfer band has been invoked by Higuchi et al.<sup>12c</sup> to explain the spectra of push–pull bithiophenes and quaterthiophenes end-capped with a methoxy group on one side and an electron-withdrawing group on the other side.

(32) Negri, F.; Zgierski, M. Z. *J. Chem. Phys.* **1994**, *100*, 2571.

(33) Rubio, M.; Merchán, M.; Ortí, E.; Roos, B. O. *Chem. Phys. Lett.* **1996**, *248*, 321.



**Figure 5.** B3LYP/6-31G\*\* one-electron energies ( $\epsilon_i$ ) diagram including the highest occupied and lowest unoccupied molecular orbitals.



**Figure 6.** Electronic density contours ( $0.03 \text{ e/bohr}^3$ ) calculated with the Molden-4 graphics interface for the frontier molecular orbitals of  $\text{PhT}_3\text{-NO}_2$  (a) and  $\text{NO}_2\text{T}_3\text{NO}_2$  (b).

(ii) The second absorption band observed at 342 nm (3.63 eV) is due to the transition to the second excited state calculated at 3.45 eV ( $f = 0.44$ ). This electronic transition mainly involves the  $\text{HOMO} \rightarrow \text{LUMO} + 1$  excitation and has a nature similar to the  $\text{HOMO} \rightarrow \text{LUMO}$  transition in  $\text{PhT}_3\text{Ph}$ ,  $\text{PhT}_3\text{Br}$ , and  $\text{BrT}_3\text{Br}$ . The band at 342 nm therefore has to be correlated with the intense band recorded for these systems at 384, 366, and 344 nm, respectively.

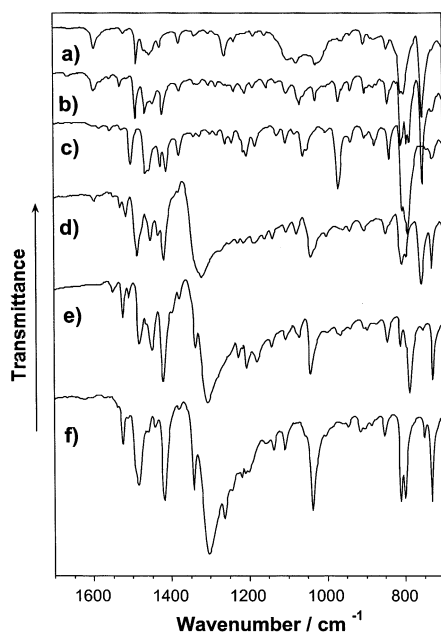
(iii) The absorption band observed at 230 nm (5.39 eV) corresponds to the  $\text{HOMO} - 1 \rightarrow \text{LUMO} + 2$  transition calculated at 5.19 eV ( $f = 0.07$ ) and has to be correlated with

the second absorption band of  $\text{PhT}_3\text{Ph}$  (264 nm),  $\text{PhT}_3\text{Br}$  (248 nm), and  $\text{BrT}_3\text{Br}$  (236 nm).

The assignment of the electronic spectrum of  $\text{BrT}_3\text{NO}_2$  is analogous to that performed for  $\text{PhT}_3\text{NO}_2$ . The most intense absorption band observed at 438 nm (2.82 eV) is associated with the  $\text{HOMO} \rightarrow \text{LUMO}$  transition calculated at 2.83 eV ( $f = 0.62$ ) and implies a charge transfer similar to that discussed for  $\text{PhT}_3\text{NO}_2$ . The second absorption band at 316 nm (3.92 eV) now results from the electronic transitions calculated at 3.71 ( $f = 0.15$ ), 3.78 ( $f = 0.14$ ), and 3.89 eV ( $f = 0.05$ ), which involve the  $\text{HOMO} \rightarrow \text{LUMO} + 1$ ,  $\text{HOMO} - 1 \rightarrow \text{LUMO}$ , and  $\text{HOMO} - 2 \rightarrow \text{LUMO}$  excitations. The large multiconfigurational character of these transitions is due to the near-degeneracy of the one-electron excitations involved.

The electronic spectrum of  $\text{NO}_2\text{T}_3\text{NO}_2$  exhibits two absorption bands at 444 and 274 nm (2.79 and 4.52 eV) and looks similar to that of  $\text{PhT}_3\text{Ph}$ . Figure 6b shows that the HOMO and LUMO of  $\text{NO}_2\text{T}_3\text{NO}_2$  spread over the whole molecule and that their atomic orbital compositions are identical to those depicted for  $\text{PhT}_3\text{Ph}$  in Figure 4. The  $\text{HOMO} \rightarrow \text{LUMO}$  transition of  $\text{NO}_2\text{T}_3\text{NO}_2$  therefore has the same nature as for  $\text{PhT}_3\text{Ph}$ ,  $\text{BrT}_3\text{-Ph}$ , and  $\text{BrT}_3\text{Br}$  and does not imply the charge-transfer calculated for  $\text{PhT}_3\text{NO}_2$  and  $\text{BrT}_3\text{NO}_2$ , for which the HOMO and LUMO are localized on different sides of the molecule. The transition is calculated to be very intense ( $f = 0.87$ ) and has an energy of 2.81 eV, in very good accord with the experiment. The low energy of the transition is due to the large stabilization of the LUMO (see Figure 5) in which the  $\text{NO}_2$  group largely participates. The low intense band at 274 nm is assigned to transitions to higher excited states calculated at 4.24 ( $f = 0.10$ ) and 4.42 eV ( $f = 0.08$ ) and has to be correlated with the second band observed for  $\text{PhT}_3\text{Ph}$  (264 nm) or  $\text{BrT}_3\text{Br}$  (236 nm) associated with the  $\text{HOMO} - 1 \rightarrow \text{LUMO} + 1$  transition.

Theoretical calculations have therefore shown that the assignment of the electronic spectrum is the same for  $\text{PhT}_3\text{Ph}$ ,  $\text{PhT}_3\text{Br}$ ,  $\text{BrT}_3\text{Br}$ , and  $\text{NO}_2\text{T}_3\text{NO}_2$ . For these molecules, the most intense absorption band corresponds to the  $\text{HOMO} \rightarrow \text{LUMO}$  one-electron promotion, the HOMO and the LUMO being delocalized over the whole molecule. The band blue-shifts as bromine atoms are added due to the stabilization of the HOMO, which enlarges the HOMO–LUMO gap, and red-shifts for



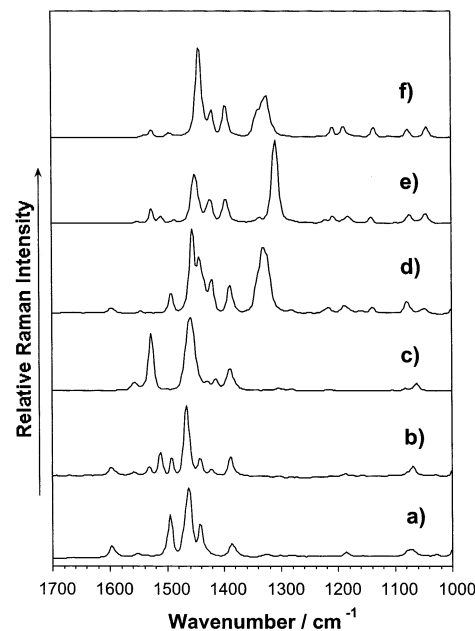
**Figure 7.** FT infrared spectra recorded for  $XT_3Y$  derivatives in solid state over probe energies of 1700–700  $\text{cm}^{-1}$ : (a)  $\text{PhT}_3\text{Ph}$ , (b)  $\text{PhT}_3\text{Br}$ , (c)  $\text{BrT}_3\text{Br}$ , (d)  $\text{PhT}_3\text{NO}_2$ , (e)  $\text{BrT}_3\text{NO}_2$ , and (f)  $\text{NO}_2\text{T}_3\text{NO}_2$ .

$\text{NO}_2\text{T}_3\text{NO}_2$  due to the stabilization of the LUMO, which narrows the HOMO–LUMO gap. For  $\text{PhT}_3\text{NO}_2$  and  $\text{BrT}_3\text{NO}_2$ , a new absorption band appears at low energies associated with a charge transfer from the electron-donor side to the electron-acceptor side of the molecule.  $\text{PhT}_3\text{NO}_2$  and  $\text{BrT}_3\text{NO}_2$  thus behave as push–pull systems with a large photoinduced polarizability. This is one of the requirements to present attractive nonlinear optical properties.<sup>34</sup>

**(c) Vibrational Spectra.** Figures 7 and 8 display the infrared and Raman spectra, respectively, and Tables 2 and 3 summarize the frequency values for the main bands. In view of the vibrational spectra some general considerations can be made:

(i) The Raman spectra present few bands and look much simpler than the infrared spectra. This observation is consistent with the existence of a long path of alternating C=C and C–C bonds, so that particular totally symmetric normal modes are selectively enhanced in the Raman spectra. We refer the reader to the existing literature on this subject.<sup>15,35,36</sup> The number of bands is, however, greater than the three or four Raman bands observed for aromatic nonpolar oligothiophenes, due to the lack of molecular symmetry and/or to the electronic interaction between the oligothiophene backbone and the end groups.<sup>16,17,37</sup>

(ii) The infrared bands associated with the  $\nu(\text{C}=\text{C})$  stretchings (i.e., those appearing in the range 1600–1400  $\text{cm}^{-1}$ ) are significantly stronger for the nitro derivatives than for aromatic nonpolar oligothiophenes.<sup>16,37</sup> For the latter, the strongest infrared bands are due to out-of-plane  $\gamma(\text{C}-\text{H})$  deformation modes and appear around 800  $\text{cm}^{-1}$ . For nitroterthiophenes, the



**Figure 8.** FT Raman spectra recorded for  $XT_3Y$  derivatives in solid state over probe energies of 1700–1000  $\text{cm}^{-1}$ : (a)  $\text{PhT}_3\text{Ph}$ , (b)  $\text{PhT}_3\text{Br}$ , (c)  $\text{BrT}_3\text{Br}$ , (d)  $\text{PhT}_3\text{NO}_2$ , (e)  $\text{BrT}_3\text{NO}_2$ , and (f)  $\text{NO}_2\text{T}_3\text{NO}_2$ .

**Table 2.** Correlation between the Vibrational Infrared Frequencies<sup>a</sup> Measured for End-Capped Terthiophenes

$\text{PhT}_3\text{Ph}$	$\text{PhT}_3\text{Br}$	$\text{BrT}_3\text{Br}$	$\text{PhT}_3\text{NO}_2$	$\text{BrT}_3\text{NO}_2$	$\text{NO}_2\text{T}_3\text{NO}_2$
1596	1596		1596		
1520	1529		1530	1524	1524
			1516		
		1502		1508	
1487	1489		1486	1482	1484
	1465	1466			
1454		1455	1453	1449	
	1444				1442
1427	1420	1427	1433	1420	1418
		1414	1418		
1377	1376	1377		1378	
1336	1336	1339		1337	1342
		1324	1322		
1301	1301	1297		1306	1304
1260		1258			1264
1236	1235	1241	1227	1220	
	1207	1203		1205	1210
1185	1186	1182	1166	1179	
1157	1152		1159		
		1125	1138	1141	1138
1097	1101	1104	1103	1105	1108
1076	1067	1080	1077	1072	
1026	1029	1050	1041	1042	1038
	936	938	941	940	946
905	902	902	904	896	914
844	842	838	848	845	852
808	808	804	807	810	810
801	793	791	796	787	800
753	753	743	757	753	750
	725	725	729	727	730

<sup>a</sup> Infrared frequencies are given in reciprocal centimeters.

$\gamma(\text{C}-\text{H})$  vibrations no longer give rise to the main absorptions, and they show a very strong and broad band around 1300  $\text{cm}^{-1}$ , which is absent for  $\text{PhT}_3\text{Ph}$ ,  $\text{PhT}_3\text{Br}$ , and  $\text{BrT}_3\text{Br}$ .

(34) (a) Bella, S. D.; Marks, T. J.; Ratner, M. *J. Am. Chem. Soc.* **1994**, *116*, 4440. (b) Varanasi, P. R.; Jen, A. K.-Y.; Chandrasekhar, J.; Nambhothiri, I. N. N.; Rathna, A. *J. Am. Chem. Soc.* **1996**, *118*, 12443.

(35) (a) Horovitz, B. *Phys. Rev. Lett.* **1981**, *47*, 1491. (b) Horovitz, B. *Solid State Commun. Colloq.* **1982**, *41*, 729.

(36) Ehrenfreund, E.; Vardeny, Z.; Brafman, O.; Horovitz, B. *Phys. Rev. B* **1987**, *36*, 1535.

(37) Hernández, V.; Muguruma, H.; Hotta, S.; López Navarrete, J. T. *J. Phys. Chem. A* **2000**, *104*, 735.

**Table 3.** Correlation between the Vibrational Raman Frequencies<sup>a</sup> Measured for End-Capped Terthiophenes

PhT <sub>3</sub> Ph	PhT <sub>3</sub> Br	BrT <sub>3</sub> Br	PhT <sub>3</sub> NO <sub>2</sub>	BrT <sub>3</sub> NO <sub>2</sub>	NO <sub>2</sub> T <sub>3</sub> NO <sub>2</sub>
1597	1599		1597		
1552	1558	1557	1546	1550	
	1532	1527	1532	1526	1526
	1511			1509	
1495	1491		1492		1495
1462	1463	1457	1454	1450	1442
1442	1442		1443		
	1422	1429	1421	1423	1420
		1414			
				1395	1396
1386	1387	1389	1388		
			1330	1336	1330
					1324
	1303	1302		1308	

<sup>a</sup> Raman frequencies are given in reciprocal centimeters.

(iii) Some vibrational normal modes are strongly active in both the infrared and Raman spectra of PhT<sub>3</sub>NO<sub>2</sub> and BrT<sub>3</sub>NO<sub>2</sub>. This phenomenon is unusual since, even in the absence of inversion symmetry, infrared and Raman spectra are complementary. In most cases, the strongest bands in the Raman are weak in infrared and vice versa. This spectroscopic behavior has been previously reported for push–pull oligoethenes and oligothiophenes.<sup>12a,38</sup>

(iv) The three nitroterthiophenes show a similar Raman profile, with the bands due to  $\nu(\text{C}=\text{C})$  stretchings (1500–1400 cm<sup>-1</sup>) being somewhat downshifted with respect to those of PhT<sub>3</sub>Ph. The NO<sub>2</sub> groups are expected to contribute significantly to the  $\pi$ -conjugation of the molecule, since the band around 1320 cm<sup>-1</sup>, which is absent in the spectra of PhT<sub>3</sub>Br, PhT<sub>3</sub>Ph, and BrT<sub>3</sub>Br, displays strong Raman activity. Similar spectral patterns are also found for the infrared spectra of PhT<sub>3</sub>NO<sub>2</sub>, BrT<sub>3</sub>NO<sub>2</sub>, and NO<sub>2</sub>T<sub>3</sub>NO<sub>2</sub>.

The infrared and Raman spectra of the six end-capped terthiophenes and of HT<sub>3</sub>H were calculated at the B3LYP/6-31G\*\* level. The spectra of HT<sub>3</sub>H and BrT<sub>3</sub>Br were first computed for both the C<sub>2</sub> and C<sub>s</sub> conformations depicted in Figure 2. Both conformations led to the same peak structures and only slight differences in frequencies and intensities were found. The theoretical frequencies quoted below thus correspond to spectra calculated for the more stable C<sub>2</sub>-type conformations summarized in Table 1.

The infrared spectra of oligothiophenes over the range 1550–1400 cm<sup>-1</sup> are dominated by two peaks due to the collective  $\nu_{\text{asym}}(\text{C}=\text{C})$  and  $\nu_{\text{sym}}(\text{C}=\text{C})$  stretchings of the thiophene rings.<sup>16,39,40</sup> The peaks respectively appear at 1497 and 1424 cm<sup>-1</sup> for unsubstituted terthiophene<sup>39</sup> and shift to 1518 and 1445 cm<sup>-1</sup> when end-capping methyl groups are added at the end  $\alpha$ -positions.<sup>16</sup> These trends are perfectly reproduced by B3LYP/

6-31G\*\* calculations, which predict wavenumbers of 1496 and 1428 cm<sup>-1</sup> for unsubstituted terthiophene and of 1520 and 1444 cm<sup>-1</sup> for  $\alpha,\alpha'$ -dimethylterthiophene.

The infrared spectra of the terthiophenes studied in this work exhibit a more complex peak structure in the 1550–1440 cm<sup>-1</sup> region due to (i) the interaction of the terthiophene backbone with the end-capping groups, (ii) the presence of the butyl chains, and (iii) the asymmetry of the compounds. For BrT<sub>3</sub>Br, the  $\nu_{\text{asym}}(\text{C}=\text{C})$  vibration is observed at 1502 cm<sup>-1</sup> (calcd 1501 cm<sup>-1</sup>), similarly to unsubstituted terthiophene. For PhT<sub>3</sub>Ph, it appears as a low-intensity peak at 1520 cm<sup>-1</sup> (calcd 1510 cm<sup>-1</sup>), and the more intense peaks at 1596 and 1487 cm<sup>-1</sup> mainly correspond to stretchings of the benzene rings. The band associated with the  $\nu_{\text{sym}}(\text{C}=\text{C})$  vibration splits in two peaks both for BrT<sub>3</sub>Br (1427 and 1414 cm<sup>-1</sup>) and for PhT<sub>3</sub>Ph (1454 and 1427 cm<sup>-1</sup>). The double-peak band observed at intermediate frequencies (1466–1455 cm<sup>-1</sup>) for BrT<sub>3</sub>Br results from bending vibrations of the C–H bonds in the butyl chains. The IR spectrum of PhT<sub>3</sub>Br mixes the features observed for PhT<sub>3</sub>Ph and BrT<sub>3</sub>Br, with the peaks associated with the  $\nu_{\text{asym}}(\text{C}=\text{C})$  and  $\nu_{\text{sym}}(\text{C}=\text{C})$  vibrations being now those observed at 1529 and 1420 cm<sup>-1</sup>, respectively.

The IR spectra of the nitro compounds present a sharp peak about 1524 cm<sup>-1</sup> that is not observed for the other derivatives. Calculations predict that this peak is due to the asymmetric stretching of the NO<sub>2</sub> groups coupled with the asymmetric stretching of the C=C bonds in the adjacent thiophene rings (see Figure 9a). For NO<sub>2</sub>T<sub>3</sub>NO<sub>2</sub>, the collective  $\nu_{\text{asym}}(\text{C}=\text{C})$  vibration depicted in Figure 9b gives rise to the intense peak recorded at 1484 cm<sup>-1</sup>. This peak appears at lower frequencies than for unsubstituted terthiophene (1497 cm<sup>-1</sup>)<sup>39</sup> due to the softening of the C=C bonds forming the conjugation path (see Table 1). The intense peak at 1418 cm<sup>-1</sup> results from the out-of-phase symmetric vibrations sketched in Figure 9c. The vibration mainly implies the outer thiophene rings and involves both the double and single CC bonds in accord with the low BLA value (0.028 Å) calculated for those rings. For the asymmetric compound PhT<sub>3</sub>NO<sub>2</sub>, the  $\nu_{\text{sym}}(\text{C}=\text{C})$  vibration splits into two peaks at 1453 and 1418 cm<sup>-1</sup>. The lowering of  $\pi$ -electron density over the nitro-substituted thiophene explains why the  $\nu_{\text{sym}}(\text{C}=\text{C})$  vibration of this subunit is measured around 1420 cm<sup>-1</sup>, a rather low value as compared with the 1450 cm<sup>-1</sup> of the phenyl subunit. The nitro derivatives present a very intense IR band around 1310 cm<sup>-1</sup>, which is largely due to the stretching of the C <sub>$\alpha$</sub> –N and N–O bonds coupled with the breathing of the adjacent thiophene rings (see Figure 9d). The high intensity of this band is due to the strong polarization of the nitro groups. For instance, the Mulliken net atomic charges calculated for the C <sub>$\alpha$</sub> , N, and O atoms in PhT<sub>3</sub>NO<sub>2</sub> are +0.02e, +0.39e, and –0.40e, respectively.

Usually, the Raman spectra of aromatic nonpolar oligothiophenes only show four bands (termed as lines A, B, C, and D) selectively enhanced with respect to the remaining Raman-active normal modes by the existence of a strong electron–phonon coupling.<sup>15,17,35,42</sup> The behavior of these four lines is as follows: (i) Line A decreases in intensity as the length of the  $\pi$ -conjugated path increases and is due to a totally symmetric

(38) Bianco, A.; Del Zoppo, M.; Zerbi, G. *Synth. Met.* **2002**, *125*, 81.

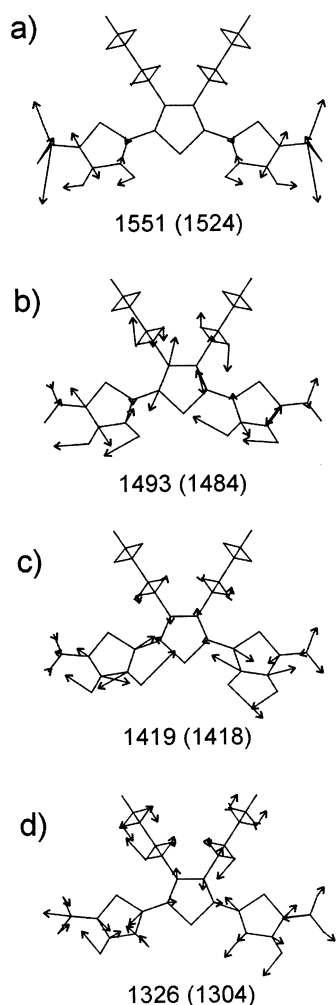
(39) (a) Harada I.; Furukawa, Y. In *Vibrational Spectra and Structure*; Durij, J. R., Ed.; Elsevier: Amsterdam, 1991; Vol. 19, p 369. (b) Furukawa, Y.; Akimoto, M.; Harada, I. *Synth. Met.* **1987**, *18*, 151.

(40) Louarn, G.; Buisson, J. P.; Lefrant, S.; Fichou, D. *J. Phys. Chem.* **1995**, *99*, 11399.

(41) Louarn, G.; Mevellec, J. Y.; Buisson, J. P.; Lefrant, S. *J. Chim. Phys.* **1992**, *89*, 987.

(42) Hernández, V.; Castiglioni, C.; Del Zoppo, M.; Zerbi, G. *Phys. Rev. B* **1994**, *50*, 9815.

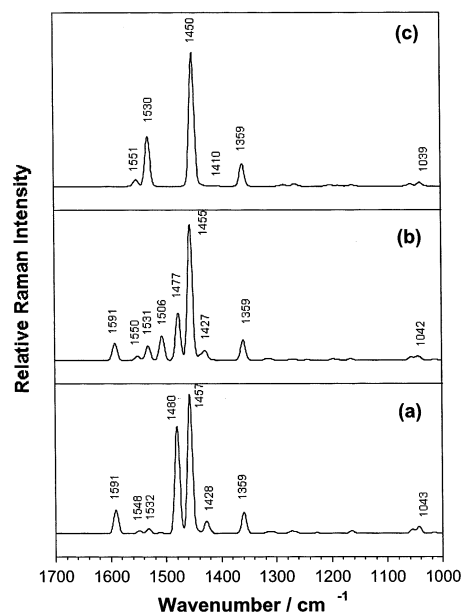




**Figure 9.** B3LYP/6-31G\*\* eigenvectors calculated for selected infrared-active vibrations of  $\text{NO}_2\text{T}_3\text{NO}_2$ . Scaled and experimental wavenumbers (in parentheses) are given in reciprocal centimeters.

$\nu_{\text{asym}}(\text{C}=\text{C})$  mode mainly located on the outer thiophene rings. (ii) Line B is always the strongest one and results from a collective totally symmetric  $\nu_{\text{sym}}(\text{C}=\text{C})$  mode in which all thiophene rings vibrate in-phase and with similar amplitudes. (iii) Line C displays an appreciable intensity only for  $\alpha$ - or  $\beta$ -substituted oligothiophenes and is also due to a collective totally symmetric  $\nu_{\text{sym}}(\text{C}=\text{C})$  mode in which the successive thiophene rings vibrate out-of-phase. (iv) Line D arises from a totally symmetric  $\delta_{\text{sym}}(\text{C}-\text{H})$  mode in which hydrogen atoms attached to all the  $\beta$ -positions of the oligothiophene vibrate in-phase. Lines A, B, C, and D are recorded at 1524, 1453, 1417, and 1045  $\text{cm}^{-1}$  for unsubstituted terthiophene<sup>39,41</sup> and shift up to 1546, 1488, 1445, and 1044  $\text{cm}^{-1}$  for  $\alpha,\alpha'$ -dimethylterthiophene.<sup>16,43</sup>

The Raman spectra of  $\text{PhT}_3\text{Ph}$  and  $\text{BrT}_3\text{Br}$  present the bands typical of aromatic nonpolar oligothiophenes but also show distinctive features. The theoretical spectra calculated for these molecules (Figure 10) are in good agreement with experiment and allow for a detailed assignment of the spectral features. For  $\text{BrT}_3\text{Br}$ , lines A, B, C, and D are observed (calculated) at 1527 (1530), 1457 (1450), 1414 (1410), and 1040 (1039)  $\text{cm}^{-1}$ , respectively (see the corresponding eigenvectors in Figure S1).



**Figure 10.** B3LYP/6-31G\*\* Raman spectra calculated for (a)  $\text{PhT}_3\text{Ph}$ , (b)  $\text{PhT}_3\text{Br}$ , and (c)  $\text{BrT}_3\text{Br}$ . Wavenumbers (in reciprocal centimeters) are indicated for the most intense peaks.

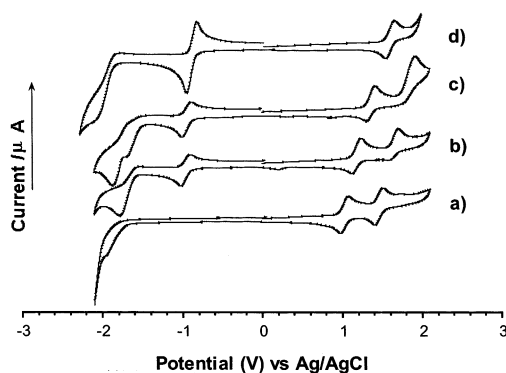
These wavenumbers are almost identical to those registered for unsubstituted terthiophene,<sup>39,41</sup> showing the small influence of the bromine atoms. For  $\text{PhT}_3\text{Ph}$ , line A is calculated at 1532  $\text{cm}^{-1}$  with a very low intensity and is almost not observed in the experiment, line B corresponds to the most intense peak at 1462  $\text{cm}^{-1}$  (calcd 1457  $\text{cm}^{-1}$ ), and line C is not distinguished. The Raman spectrum of  $\text{PhT}_3\text{Ph}$  furthermore presents a low-intensity band at 1597  $\text{cm}^{-1}$  (calcd 1591  $\text{cm}^{-1}$ ) and an intense band at 1495  $\text{cm}^{-1}$  (calcd 1480  $\text{cm}^{-1}$ ). These bands were also observed in the IR spectrum and arise from benzene stretchings, as is also the case for the band at 1442  $\text{cm}^{-1}$ .

The Raman spectrum of  $\text{PhT}_3\text{Br}$  is almost a superposition of the spectra of  $\text{PhT}_3\text{Ph}$  and  $\text{PhT}_3\text{Br}$ . The peaks at 1599, 1491, and 1442  $\text{cm}^{-1}$  correspond to stretchings of the phenyl groups; line A is observed at 1532  $\text{cm}^{-1}$  (two other  $\nu_{\text{asym}}(\text{C}=\text{C})$  vibrations are seen at 1558 and 1511  $\text{cm}^{-1}$ ), line B appears at 1463  $\text{cm}^{-1}$ , and line C occurs at 1422  $\text{cm}^{-1}$ . All three molecules present a medium-intensity band at ca. 1385  $\text{cm}^{-1}$  (not observed for terthiophene and  $\alpha,\alpha'$ -dimethylterthiophene) due to a vibration mainly describing the stretching of the central  $\text{C}_\beta-\text{C}_\beta$  bond bearing the butyl chains.

The assignment of the spectra of the nitro derivatives follows similar patterns. Line A appears as a low-intensity peak at 1526  $\text{cm}^{-1}$  for  $\text{NO}_2\text{T}_3\text{NO}_2$  and  $\text{BrT}_3\text{NO}_2$  and at 1532  $\text{cm}^{-1}$  for  $\text{PhT}_3\text{-NO}_2$ . Line B corresponds to the intense peaks observed at 1454 ( $\text{PhT}_3\text{NO}_2$ ), 1450 ( $\text{Br}_2\text{T}_3\text{NO}_2$ ), and 1442  $\text{cm}^{-1}$  ( $\text{NO}_2\text{T}_3\text{NO}_2$ ). Line C is recorded around 1420  $\text{cm}^{-1}$  for the three compounds, and the peak at about 1390  $\text{cm}^{-1}$  corresponds to the stretching of the central  $\text{C}_\beta-\text{C}_\beta$  bond. The lines near 1330  $\text{cm}^{-1}$  are due to the  $\nu(\text{C}_\alpha-\text{N})$  stretchings and are very strong, which further confirms the extension of the  $\pi$ -conjugation to the  $\text{NO}_2$  groups.

The vibration that gives rise to line B (the ECC mode) has a collective character since it spreads over the whole  $\pi$ -conjugated backbone. Along this vibration, all the alternating  $\text{C}=\text{C}$  bonds lengthen in-phase while all the  $\text{C}-\text{C}$  bonds shrink in-phase. This characteristic normal mode is strongly coupled to the movement of the  $\pi$ -electrons, and its associated eigenvector resembles the

(43) Casado, J.; Hernández, V.; Hotta, S.; López Navarrete, J. T. *J. Chem. Phys.* **1998**, *109*, 10419.



**Figure 11.** Cyclic voltammograms of (a) PhT<sub>3</sub>Br, (b) PhT<sub>3</sub>NO<sub>2</sub>, (c) BrT<sub>3</sub>NO<sub>2</sub>, and (d) NO<sub>2</sub>T<sub>3</sub>NO<sub>2</sub> in 0.1 M TBAPF<sub>6</sub>/CH<sub>2</sub>Cl<sub>2</sub>, scan rate = 100 mV/s.

**Table 4.** Electrochemical Data<sup>a</sup> for End-Capped Terthiophenes

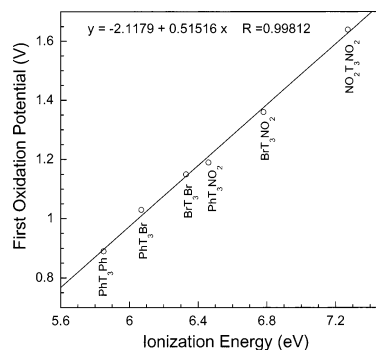
	oxidation processes		reduction processes	
	$E^{o'}_1$ (V)	$E^{o'}_2$ (V)	$E^{o'}_1$ (V)	$E^{o'}_2$ (V)
PhT <sub>3</sub> Ph <sup>b</sup>	0.89	1.29		
PhT <sub>3</sub> Br	1.03	1.47		
BrT <sub>3</sub> Br	1.15	1.68		
PhT <sub>3</sub> NO <sub>2</sub>	1.19	1.72 <sup>c</sup>	-0.96	-1.77 <sup>d</sup>
BrT <sub>3</sub> NO <sub>2</sub>	1.36	1.91 <sup>c</sup>	-0.96	-1.70, <sup>d</sup> -1.88 <sup>d</sup>
NO <sub>2</sub> T <sub>3</sub> NO <sub>2</sub> <sup>e</sup>	1.64		-0.84	-2.06 <sup>d</sup>

<sup>a</sup> Measured at room temperature in a 0.1 M TBAPF<sub>6</sub>/CH<sub>2</sub>Cl<sub>2</sub> solution, scan rate = 100 mV/s. <sup>b</sup> Values from ref 22a. <sup>c</sup> Irreversible process,  $E_{pa}$  value provided. <sup>d</sup> Irreversible process,  $E_{pc}$  value provided. <sup>e</sup> Values from ref 22c.

changes in bond lengths that take place in the  $\pi$ -conjugated path upon modification of the electronic structure of the molecule by chemical doping or photoexcitation. Commonly, line B shifts downward either upon chain elongation<sup>16</sup> or on going from an aromatic structure of the  $\pi$ -conjugated backbone to a quinonoid one.<sup>43,44</sup> For the terthiophenes studied here, line B downshifts by 20 cm<sup>-1</sup> upon nitro substitution of the end  $\alpha$ -positions (PhT<sub>3</sub>-Ph, 1462 cm<sup>-1</sup>; PhT<sub>3</sub>NO<sub>2</sub>, 1454 cm<sup>-1</sup>; BrT<sub>3</sub>NO<sub>2</sub>, 1450 cm<sup>-1</sup>; NO<sub>2</sub>T<sub>3</sub>NO<sub>2</sub>, 1442 cm<sup>-1</sup>), thus supporting a certain degree of quinonoid character of the terthiophene backbone due to the strength of the electron-withdrawing NO<sub>2</sub> groups.

**(d) Electrochemical Data.** Figure 11 shows the cyclic voltammograms (CVs) recorded for PhT<sub>3</sub>Br, PhT<sub>3</sub>NO<sub>2</sub>, and BrT<sub>3</sub>NO<sub>2</sub>. The CV reported previously for NO<sub>2</sub>T<sub>3</sub>NO<sub>2</sub> is also depicted for the sake of comparison.<sup>22c</sup> The electrochemical data are summarized in Table 4.

The nitro compounds exhibit two reduction processes, while no reduction is observed for the phenyl- and bromine-substituted compounds under the experimental conditions (with the exception of PhT<sub>3</sub>Br, which displays a cathodic process near the electrolyte limit). For the mononitro derivatives, the first process corresponds to a reversible one-electron reduction and mainly involves the nitro environment on which the LUMO orbital is concentrated (see Figure 6a). UB3LYP/6-31G\*\* calculations for PhT<sub>3</sub>NO<sub>2</sub><sup>-</sup> indicate that the nitrothiophene subunit accommodates 0.47 extra electrons in the reduction process and that the nitro group accumulates a charge of -0.67e for the anion. For the dinitro derivative, the first reduction implies a reversible two-electron process in accord with the presence of two nitro



**Figure 12.** Variation of the first oxidation potential with the adiabatic ionization energy calculated at the B3LYP/6-31G\*\* level.

groups. Calculations predict that each NO<sub>2</sub> group in NO<sub>2</sub>T<sub>3</sub>NO<sub>2</sub><sup>2-</sup> has a charge of -0.80e and that each nitrothiophene subunit incorporates 0.78 extra electrons in the reduction process. Reduction indeed affects the whole terthiophene backbone because, as depicted in Figure 6b, the LUMO of NO<sub>2</sub>T<sub>3</sub>NO<sub>2</sub> spreads over the three thiophene rings. Furthermore, calculations show that, upon reduction to the dianion, the molecule becomes fully planar and the three thiophene rings undergo a reversal of the single-double CC bond alternation pattern, reaching a quinonoid structure. The lengths of the C <sub>$\alpha$</sub> -C <sub>$\beta$</sub>  bonds (C3-C4 and C5-C6, 1.434 Å) are longer than those of the C <sub>$\alpha$</sub> -C <sub>$\alpha$</sub>  bonds (C4-C5, 1.392 Å) and C <sub>$\beta$</sub> -C <sub>$\beta$</sub>  bonds (C2-C3, 1.377 Å; C6-C7, 1.394 Å).

The second reduction process is irreversible on the CV time scale and completes the reduction of the terthienyl backbone for PhT<sub>3</sub>NO<sub>2</sub> and BrT<sub>3</sub>NO<sub>2</sub>. For NO<sub>2</sub>T<sub>3</sub>NO<sub>2</sub>, it shifts to more negative potentials due to the strong on-site Coulombic repulsion to accommodate the introduction of a third electron.

All six terthiophenes, including the dinitro derivative, present a first oxidation process that is reversible and leads to the formation of stable radical cations (see Table 4). The oxidation potential recorded for BrT<sub>3</sub>Br (1.15 V) is similar to those reported for  $\beta$ -substituted  $\alpha,\alpha'$ -terthiophenes,<sup>45</sup> supporting the small effect of the bromine atoms. The potential decreases upon going to PhT<sub>3</sub>Ph (0.89 V), due to the extension of the conjugation path, and increases upon nitro substitution (1.64 V for NO<sub>2</sub>T<sub>3</sub>NO<sub>2</sub>) reflecting the destabilization effect of the electron-withdrawing nitro groups. The UB3LYP/6-31G\*\* calculations performed for the cations indicate that the oxidation process mainly involves the terthienyl moiety that becomes partially quinoidized.

Figure 12 shows the linear correlation found between the first oxidation potential, measured experimentally, and the adiabatic ionization energy, calculated as the energy difference between the optimized structures of the cation and the neutral molecule. This correlation can be used as a theoretical tool to predict the oxidation potentials of new end-capped terthiophenes incorporating electron-releasing or electron-withdrawing groups different from those employed here. A correlation between the frequency of the ECC mode (line B) and the first oxidation potential is also evident. The downshift of the former is associated with an increment of the electron-deficient character of the terthienyl moiety and therefore with an increase of the energy required to extract the electron.

(44) Hernández, V.; Hotta, S.; López Navarrete, J. T. *J. Chem. Phys.* **1998**, *109*, 2543.

(45) Bäuerle, P. In ref 10a, p 105.

PhT<sub>3</sub>Ph, PhT<sub>3</sub>Br, and BrT<sub>3</sub>Br present a reversible second oxidation process that corresponds to the generation of the dication. The process becomes irreversible for PhT<sub>3</sub>NO<sub>2</sub> and BrT<sub>3</sub>NO<sub>2</sub> and is not observed for NO<sub>2</sub>T<sub>3</sub>NO<sub>2</sub>, in accord with the electron-deficient character of the terthiophene backbone. The B3LYP/6-31G\*\* calculations performed for BrT<sub>3</sub>Br<sup>2+</sup>, as an illustrative example, show that the structure of the dication is planar and fully quinoidized. The C<sub>α</sub>–C<sub>α'</sub> and C<sub>β</sub>–C<sub>β</sub> bonds are shorter (C2–C3, 1.377 Å; C4–C5, 1.395 Å; C6–C7, 1.389 Å) than the C<sub>α</sub>–C<sub>β</sub> bonds (C1–C2, 1.409 Å; C3–C4, 1.431 Å; C5–C6, 1.452 Å).

#### IV. Conclusions

A series of 3',4'-dibutylterthiophenes (XT<sub>3</sub>Y) bearing phenyl, bromine, and nitro groups at the end α,α'-positions have been investigated by using UV–vis, infrared, and Raman spectroscopies together with cyclic voltammetry and DFT theoretical calculations. The structural, electronic, vibrational, and redox properties of these compounds have been shown to be largely influenced by the nature of the end-capping groups, which interact with the π-conjugated terthiophene backbone.

For neutral oligomers, the terthiophene moiety is predicted to present transoid structures slightly twisted from planarity. Nitroencapsulation (NO<sub>2</sub>T<sub>3</sub>NO<sub>2</sub>) reduces the CC bond length alternation along the conjugated backbone and leads to a more delocalized, partially quinoidized structure as observed in the experimental studies.<sup>22c</sup> For the asymmetric derivatives PhT<sub>3</sub>NO<sub>2</sub> and BrT<sub>3</sub>NO<sub>2</sub>, the terthiophene bridge shows two well-differentiated structural domains, one purely aromatic and the other partially quinoidized.

The nitro derivatives are synthesized as deep red solids due to the intense absorption they present around 450 nm. This absorption is assigned to the HOMO → LUMO electronic transition, which, in the case of PhT<sub>3</sub>NO<sub>2</sub> and BrT<sub>3</sub>NO<sub>2</sub>, implies a charge transfer from the electron-donor phenyl or bromine subunit to the electron-acceptor nitro subunit. PhT<sub>3</sub>NO<sub>2</sub> and BrT<sub>3</sub>NO<sub>2</sub> behave as push–pull systems with an intense photo-induced intramolecular charge transfer. For NO<sub>2</sub>T<sub>3</sub>NO<sub>2</sub>, the HOMO and LUMO spread over the whole molecule and the HOMO → LUMO transition corresponds to the π–π\* band observed for oligothiophenes.

The infrared and Raman spectra have been comprehensively assigned on the basis of theoretical calculations. The vibrational features of the terthiophene skeleton have been identified and their evolution upon end-capping substitution has been clearly established. The frequency of the collective ECC vibration mode is observed to downshift upon nitro substitution, thus supporting the more efficient π-electron delocalization achieved for the nitro derivatives.

Cyclic voltammetry results show that PhT<sub>3</sub>NO<sub>2</sub> and BrT<sub>3</sub>NO<sub>2</sub> exhibit a dual electrochemical behavior. On one hand, they

are reduced to the anion and dianion due to the presence of the nitro groups. On the other hand, they form stable cations and even dications due to the oxidation of the terthiophene backbone, which becomes planar and fully quinoidized. The NO<sub>2</sub>T<sub>3</sub>NO<sub>2</sub> molecule also forms stable anions and cations, but the first reduction process now leads directly to the dianion. This dual redox behavior as electron acceptors and electron donors has been previously reported for thiophene derivative compounds (α-4-[bis(4-methylphenyl)amino]phenyl-α'-(dimesitylboryl)thiophene and α-4-[bis(9,9-dimethylfluorenyl)amino]phenyl-α'-(dimesitylboryl)thiophene<sup>46</sup>) and makes these compounds of great interest for the design of transistor devices owing to their potential capability of acting as n- and p-channel conductors. With this target in mind, more work is underway.

From a material science standpoint, this paper provides structural, optical, and electrochemical data that are of great interest to understand the electronic behavior in the solid state (charge injection, transport properties, optical excitations, etc.) of thiophene oligomers as a function of end-capping substituents. The oligothiophene skeleton has been shown to play an important role in stabilizing both negative and positive charges, which in turn gives rise to relatively highly delocalized charged structures. This delocalization and the large involvement of the thiophene rings in the frontier orbitals, which promotes the interaction of these orbitals between nearest neighbors, are requirements to obtain efficient charge migration in solid-state devices.

**Acknowledgment.** The research at the Universities of Málaga and Valencia was supported by the Ministerio de Ciencia y Tecnología (MCyT) of Spain through the projects BQU2000-1156 and PB98-1447, respectively. The group at Valencia acknowledges the Generalitat de Valencia for financial support (GR01-145 and XT01-5). The group of Málaga is indebted to Junta de Andalucía (Spain) for funding their research group (FQM-0159). The group at Minnesota acknowledges the NSF. We thank David D. Graff and Eric J. Hukkanen for helping in the synthesis of some of the compounds. J.C. is grateful to the Ministerio de Ciencia y Tecnología of Spain for a Ramón y Cajal position of Chemistry at the University of Málaga.

**Supporting Information Available:** Figure S1, displaying the B3LYP/6-31G\*\* eigenvectors calculated for the most intense Raman-active vibrations of BrT<sub>3</sub>Br to illustrate the normal modes involved in the main bands, with scaled and experimental (in parentheses) wavenumbers given in reciprocal centimeters (PDF). This information is available free of charge via the Internet at <http://pubs.acs.org>.

JA027835P

(46) Shirota, Y.; Kinoshita M.; Noda T.; Okumoto, K.; Ohara, T. *J. Am. Chem. Soc.* **2000**, *122*, 11021.